Numerical simulation of the noise radiated by free hot supersonic twin jets

Julien Troyes, François Vuillot

Numerical simulation of the noise radiated by free hot supersonic twin jets

J. Troyes[1]
ONERA, University of Toulouse, F-31055, Toulouse, France

F. Vuillot[2]
ONERA, University of Paris-Saclay, F-91123, Palaiseau, France

Numerical simulation of the noise radiated by free hot supersonic twin jets is conducted by combining different numerical tools. These are based on the one hand on a high fidelity LES (Large Eddy Simulation) computation with geometric triggering of the turbulence in the nozzle convergents and on the other hand on the use of a CAA code, coupled with the CFD code, to properly propagate at a lower cost the high level acoustic waves from the jet near field towards the far field microphones. This methodology has demonstrated its benefits by producing very satisfactory results. Numerical velocity profiles are shown in very good agreement with the experimental measurements for several diameters downstream of the nozzle outlets. These results show that marked interactions between the two jets only occurs several diameters after the nozzle outlets. Regarding acoustics, the results are very encouraging. Considering the far field OASPL, the numerical vs. experimental deviation ranges from 0 to 3 dB. Higher levels in the azimuths perpendicular to the two jets with respect to the levels in the azimuths coplanar to the two jets are well recovered by the computation. These higher levels do not exactly reach the theoretical addition of two single jets noise, which suggests that acoustics source efficiency is reduced by interaction effects while lower levels in the coplanar plane traduce a probable masking effect.

I. Introduction

During a launcher lift-off, the propulsive jets generate high acoustic levels which induce high loads on the launch pad infrastructure and on the launcher and its payload. Indeed, these harsh conditions, which result from strongly supersonic (M> 3), hot (3000 K), non adapted jets and with a chemical composition distinct from that of the ambient air, are sizing elements during the design of the launcher and the launchpad. Many space launcher first stages are composed of multiple engines and then, aeroacoustic interaction between hot supersonic jets is a key point.

While semi empirical methods provide affordable jet noise estimation, these have been gradually replaced by unsteady numerical simulations that allow detailed information on the acoustic sources near field. With the increase of computational ability, Large Eddy Simulation (LES) are now used broadly [1]. In order to get the far field acoustic map, integral methods have been widely used. Nevertheless, assumption required (homogeneous propagation medium and linear acoustic regime) are not always verified. For instance, space rocket noise high levels (over 160 dB) makes it mandatory to consider nonlinear propagation. Then, the use of a solver resolving the full Euler equation is a relevant option. One-way CFD/CAA method can be adequate when the propagation medium is free of obstacles or homogeneous; otherwise, two-way coupling is appropriate. A large insight on these topics is available in [2].

For a single supersonic choked jet, noise has three components. The first two are due to turbulent mixing: largest structures radiates Mach waves (which are amplified if considered jet is hot [3]) emitted at preferred angles, mainly in downstream direction, while finest ones radiate mainly in transverse and upstream directions. The third one is a consequence of the interaction of turbulence with shock cells, called Broadband Shock Associated Noise (BBSAN), which radiates mainly also in transverse and upstream directions. A fourth component, supersonic plume resonance (known as screech noise) may also occur under certain conditions.

[1] Research scientist, Multi-physics for Energetics Department, julien.troyes@onera.fr.
[2] Research scientist, Multi-physics for Energetics Department.

Regarding twin jets noise, two effects have to be accounted for: the turbulent mixing of the jets and the acoustic shielding due to steady surrounding flow. Kantola [4] experimentally links their influence with the nozzle spacing. When spacing is large, turbulent mixing is minimal, while acoustic shielding is dominant. When nozzles are close, turbulent mixing is enhanced and acoustic shielding is minimal. From basic acoustic power consideration, taking into account two jets leads to multiplying by two the power of a single jet, *i.e.* to add $10\log_{10}(2) = 3$ dB to the OASPL. Kantola reports that acoustic shielding is the greatest in the plane containing the nozzles compared to the perpendicular plane, where it is nearly vanishing. In the first plane, the OASPL addition is always smaller than 3 dB, decreasing as spacing is increasing until $3D_j$. In the second plane, the OASPL addition may be smaller than 3 dB (due to some mixing noise suppression) or greater than 3 dB (due to additional noise generation by jet interactions). Further shielding phenomena details can be found in [5].

Following Kantola's pioneering work, supersonic twin jets related studies appear in late 80's in the military field, involving fighter aircrafts using two propulsive engines. Screech phenomenon suppression is then the main effort with lots of experimental studies [6][7][8][9][10][11], of which Raman presents a synthesis [12]. In parallel, nozzle spacing effects on the three regions (converging, merging, and combining) of the flowfield are investigated by Mustapha [13], or on shielding and interaction by Bozak [14] or Osawa [15] (on a shock free jet for the latter). In the last 5 years, twin jets screech is still a research field. Coupling modes are investigated experimentally by Kuo [16], Knast [17] or Bell [18]. On this topic, numerical simulations of previous studies start to arise (Goparaju [19] on Kuo's setup [16], Gao [20] or Anh [21] on Walker's setup [10]). Finally, the main recent numerical contribution to the phenomenology of acoustic shielding and interaction is due to Pineau and Bogey [22]. They compare three spaced twin jets (ranging from $2D_j$ to $2.8D_j$) with the same single jet. Considered jets have an exit Mach number of 3.1 and a stagnation temperature of 2000 K, which are conditions required for space application studies. Kantola's conclusions are confirmed. In particular, additional interaction noise is found to be generated for broadband shock-associated noise component and for the noise radiated at low polar angles in the jet midplane.

The present study aims at comparing numerical simulation of hot supersonic twin jets in a free jet configuration with acoustic and PIV measurements carried out by Pprime laboratory of the University of Poitiers. Numerical framework relies on LES which is 2-way coupled with CAA solver for full Euler equations.

The present paper is organized as follows. The experimental setup is first presented in section II. Then, the computational domain and mesh are described in section III. In section IV, the numerical procedures are detailed. Finally, numerical results including aerodynamic and acoustic are compared to experimental results and discussed in section V.

II. Test case

The jet configuration for this test case [23] uses twice the same nozzle (exit nozzle diameter D_j) as previous studies [24], [25], integrated in an assembly that has to be adapted from the one designed for single jet. To construct the numerical test case, the single jet nozzle was duplicated, then the two nozzles were inserted in the twin jet assembly (see Figure 1) thus producing a CAD definition permitting the construction of the computational mesh. The nozzle center distance is equal to $s=2.8\ D_j$. The gas generator is mounted in the MARTEL [26] test hall at $50\ D_j$ from the ground (distance between the nozzle outlet plane and the ground).

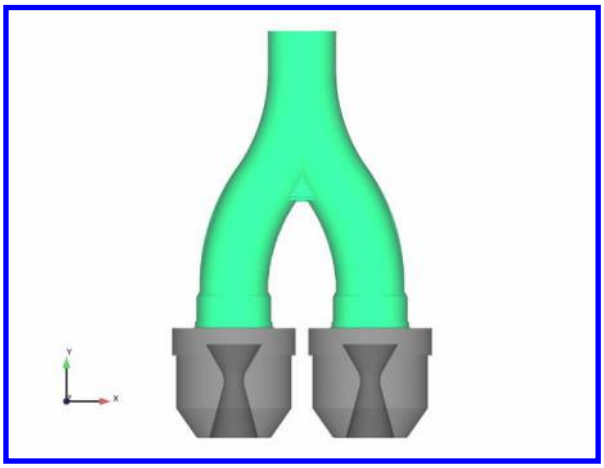

Figure 1: twin jets assembly CAD

Two kinds of measurements [27], performed by Pprime team operating at MARTEL bench, are available for this free jet configuration: PIV and acoustic. The jet generating conditions differ in temperature depending on the type of measurements carried out while pressure stays the same. Stagnation temperature T_i is 200 K higher for acoustic tests than for PIV. Furthermore, T_i for each nozzle are recorded via thermocouples upstream of the

nozzles. They are slightly different by 100 K depending on the nozzle considered ($T_{i2}>T_{i1}$). All theoretical aerodynamic and acoustic characteristics of the single jet at acoustic operating conditions are available in [28].

Regarding the PIV measurements, the time averaged velocity field is characterized in the longitudinal plane of symmetry containing the axes of the two jets. Axial coverage of developing flow varies from 0 to 42 D_j and main uncertainties are due to the positions of laser planes and of the camera.

Concerning acoustic, the microphone instrumentation is as follows (the positions are given relatively to the nozzle outlets):

- Upstream of the jet, around the generator: 3 rings G3 (h = 2.5 D_j), G4 (h = 25.16 D_j), G5 (h = 22.16D_j), composed of microphones located on circle of radius r = 5.25 D_j (centered on the axis of each nozzle for G3, on the symmetry line for G4 and G5). Based on the height h, G3 is located in the near field, while G4 and G5 are in far field.
- In the far field, 4 polar antennas (azimuth φ), located at r = 25 D_j centered at the symmetry point of the nozzle outlets. They cover a polar arc θ between 30° and 110° (angles are measured from the downstream direction). They are equipped with 3 to 7 microphones and positioned in both longitudinal planes: coplanar (φ = 0; 180°) and perpendicular (φ = 90; 270°) to the twin jets.

Ambient conditions for outside air are denoted p_{atm} and T_{atm}.

III. Computational domain and grid

The gas generator and the twin jets support integrating the two nozzles are included in a cylindrical computational domain of radius r = 33.33 D_j and total height 91.66 D_j. The origin of the calculation axes is set on the nozzles exit plane at the symmetry point, the Oy axis pointing upward. The domain extends to 41.66 D_j towards the top and 50 D_j towards the bottom.

The domain is divided into 4 user domains or zones (see Figure 2):

- Nozzle1 (in blue)
- Nozzle2 (in yellow)
- Main (in green): truncated cone
- Prop (in pink), complementary to the 3 previous ones

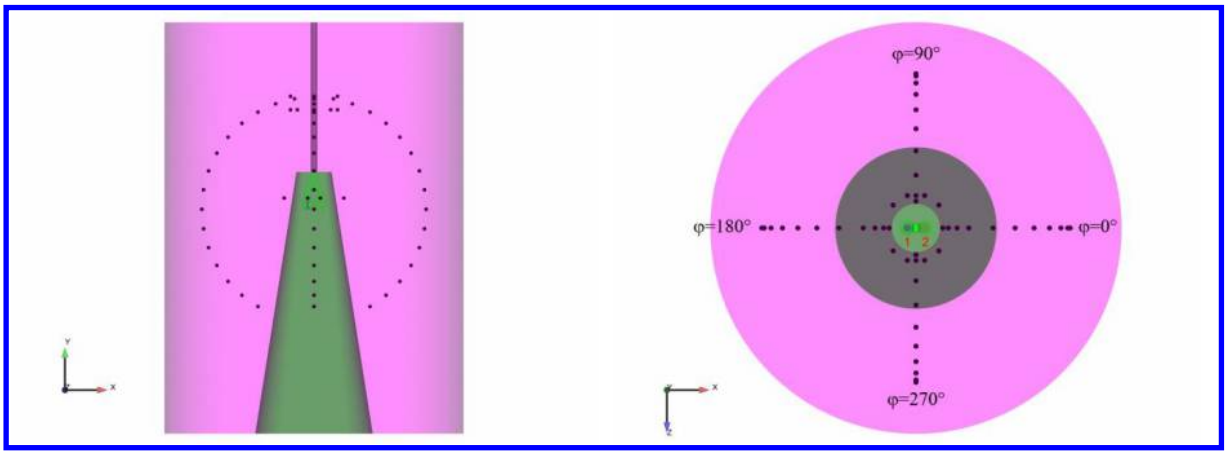

Figure 2: computational domain and microphones (left: front view, right: top view)

The first 3 zones are treated with the LES code at second order in space and time while the fourth one is devoted to the CAA code at the fourth order in space. The generated mesh is made up of three kinds of elements: tetra4, pyra5 and penta6. The prisms (penta6) are located at walls (nozzles, lips). Core regions are filled with tetrahedra, while pyramids allow to link prisms lateral faces to tetrahedra in specific conditions. As in previous studies [24], [25], a geometric step is inserted in each nozzle convergent in order to trigger fluctuating velocity levels at their exhausts. Table 1 summarizes element distribution for the whole 181 642 204 cells grid.

Table 1 : cells distribution

	Tetra4	Pyra5	Penta6	Total
Nozzle1	16 499 849	36 047	16 153 827	32 689 723
Nozzle2	16 508 923	36 135	16 142 044	32 687 102
Main	95 022 567	14 276	433 368	95 470 211
Prop	20 795 168	0	0	20 795 168

The numerical cut-off Srouhal number is linked to the number of points per wavelength (PPW) necessary to correctly propagate acoustic waves. For a second order code, it is estimated that PPW should be higher than 20, while the PPW can be reduced to 5 for a fourth order code. In the Main zone (apart from axis or lipline refinements), the tetra edge size is set to 0.100 D_j, leading to a cut-off Strouhal number of St_c=0.25 for a second order resolution. It is respectively 0.367 D_j and 0.27 for the propagative (Prop) zone for a fourth order resolution. Furthermore, the azimuthal resolution at the nozzle exit liplines is close to 2200 cells. All these characteristics are based on Δ, representing the cell equivalent diameter (Δ=edge/√6 for a regular tetrahedron).

For instance, Figure 3 displays the cell length scale Δ in z=0 plane, containing the two jets ("jets plane"), and y=G3 plane. On this figure, the spacing between two gray lines is $5D_j$.

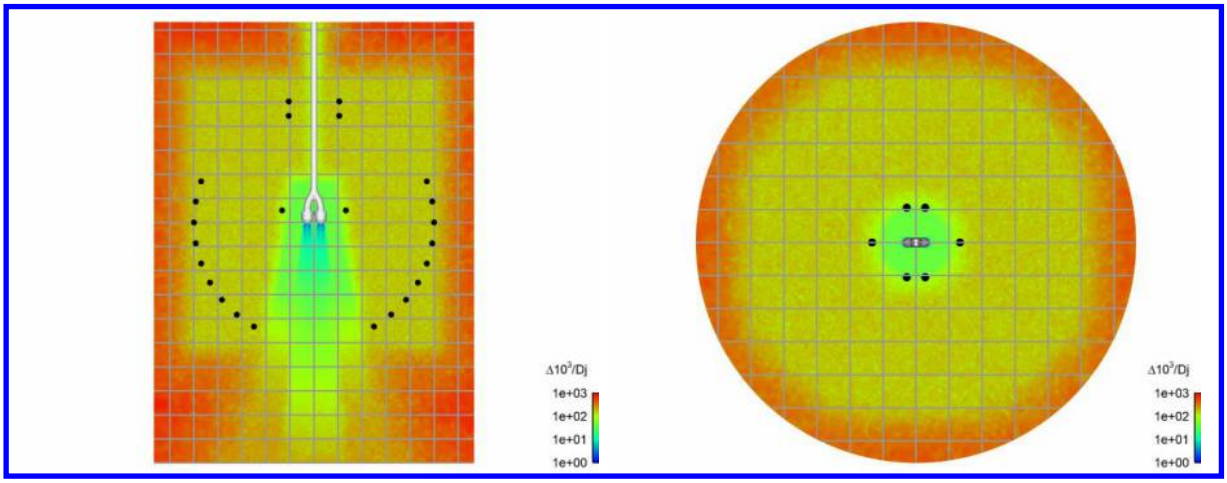

Figure 3: mesh and microphones visualization in jets plane (left), y=G3 plane (right)

The mesh is identical in the transverse planes (x = constant) of the two jets ("midplane"). All microphones are located in the propagation zone. However, due to the transition between the Main and the Prop domains, the G3 mics are located in a slightly more refined area than the other ones.

IV. Computation characteristics

The LES computation is performed with CEDRE [29], [30], using a second order spatial scheme for flow and source production (Nozzle1, Nozzle2 and Main domains), while the CAA computation is performed with SPACE [31] using a spatial scheme up to fourth order for acoustic propagation (Prop domain). The CFD code relies on a finite volume method, while the CAA one on a discontinuous Galerkin formulation and solves the full (nonlinear) Euler equations. These two solvers are two-way coupled at their interface ([24], [25], [32]). The cell localization and the data exchanges are handled by the CWIPI [33] coupling library. Both solvers are second order in time, with same global time step Δt. It must be pointed out that time integration is performed with an implicit scheme for CFD while CAA uses an explicit one. Two species are taken into account for CFD solver: air and burnt gases (also referred to as "propellant"), whereas only air is considered for CAA solver.

Boundary conditions are as follows:

- Nozzle inlets (CFD): p_i, T_i, $Y=Y_{prop}$
- Ground (CFD): relaxed subsonic outlet at p_{atm}
- Ground and all external surfaces (CAA): non-reflective
- Gas generator (CFD/CAA): adiabatic walls
- CFD/CAA: interface

Note that the choice is made to apply the same total temperature (from PIV operating conditions) T_{i2} at the inlet of the two nozzles. Moreover, the ground is treated as an exit, with the aim of avoiding recirculations. This choice is justified by the fact that ground is located 50 D_j from the nozzle outlets and therefore it does not affect the aerodynamics of the jets. Likewise, in order to avoid recirculation close to the nozzle outlets, a coflow along axial direction is applied, with V_y=-5 m/s. Initial conditions are T_{atm} and p_{atm}, with $Y=Y_{air}$ and V_y=-5 m/s.

As indicated before, the goal is to use the high-order capability of the CAA solver to precisely (and inexpensively) propagate generated high level acoustic waves to far field microphones. Nevertheless, order should be reduced in particular in zones like interface, walls, outlets for robustness and CPU cost. Such process is performed with an order-mapping feature. For instance, Figure 4 displays the order map applied in z=0 plane embedding the 2 jets and in the y=G3 plane.

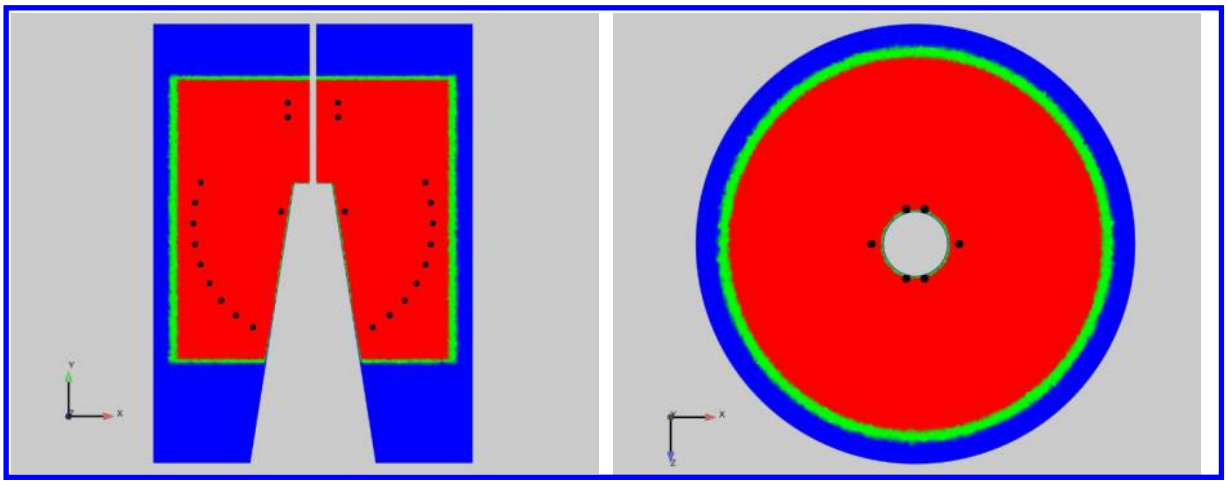

Figure 4: order-mapping visualization in z=0 plane (left), y=G3 plane (right). Red is 4th order, green 3rd order, blue 2nd order.

Like mentioned previously for mesh, G3 mics exhibit particular handling: due to their oval distribution, centered on each axis of the nozzles, the microphones at 90° and 270° are very close to the 4th-3rd order transition zone, while the microphones at 0° and 180° are entirely positioned in 4th order zone.

In addition, the arcs of experimental mics at the 4 azimuths were extended up to θ=170° upstream (not shown on Figure 3 and Figure 4). These sensors are always located in the 4th order area.

V. Results

After a transitional phase to establish the jets in the domain, all field variables and pressure signal are recorded at each time step Δt during the established phase that lasts for 1250 D_j/U_j. This represents 319 h elapsed time on 2464 Broadwell type processors (2112 for CFD and 352 for CAA).

A. Aerodynamics

First, global convergence of the established phase in the CFD domains is checked looking at averaged flow rates through boundaries as reported in Table 2.

Table 2: species flow rate through BC (kg/s)

	Inlet 1	Inlet 2	Interface	Ground
Air	0.000	0.000	46.778	-46.461
Propellant	1.265	1.265	-0.034	-2.519
Total	1.265	1.265	46.745	-48.980

The sum of the flow rates is almost zero (difference of 0.6 %). At the interface, the flow rate of the propellant species is very low. Main contribution is from air sucked through the interface and exiting through the ground boundary, considered as a flow outlet.

Instantaneous flow

For jets plane (z=0) and the three jets midplanes (x=cst), snapshots of static temperature, vorticity and static pressure in Main zone, are displayed in Figure 5 to Figure 7. Whole domain, extending to $50D_j$ after nozzles exit plane is depicted for jets plane, while a zoom of the first $15D_j$ after nozzle exit is isolated for midplanes. The spacing between two grey lines is $5D_j$.

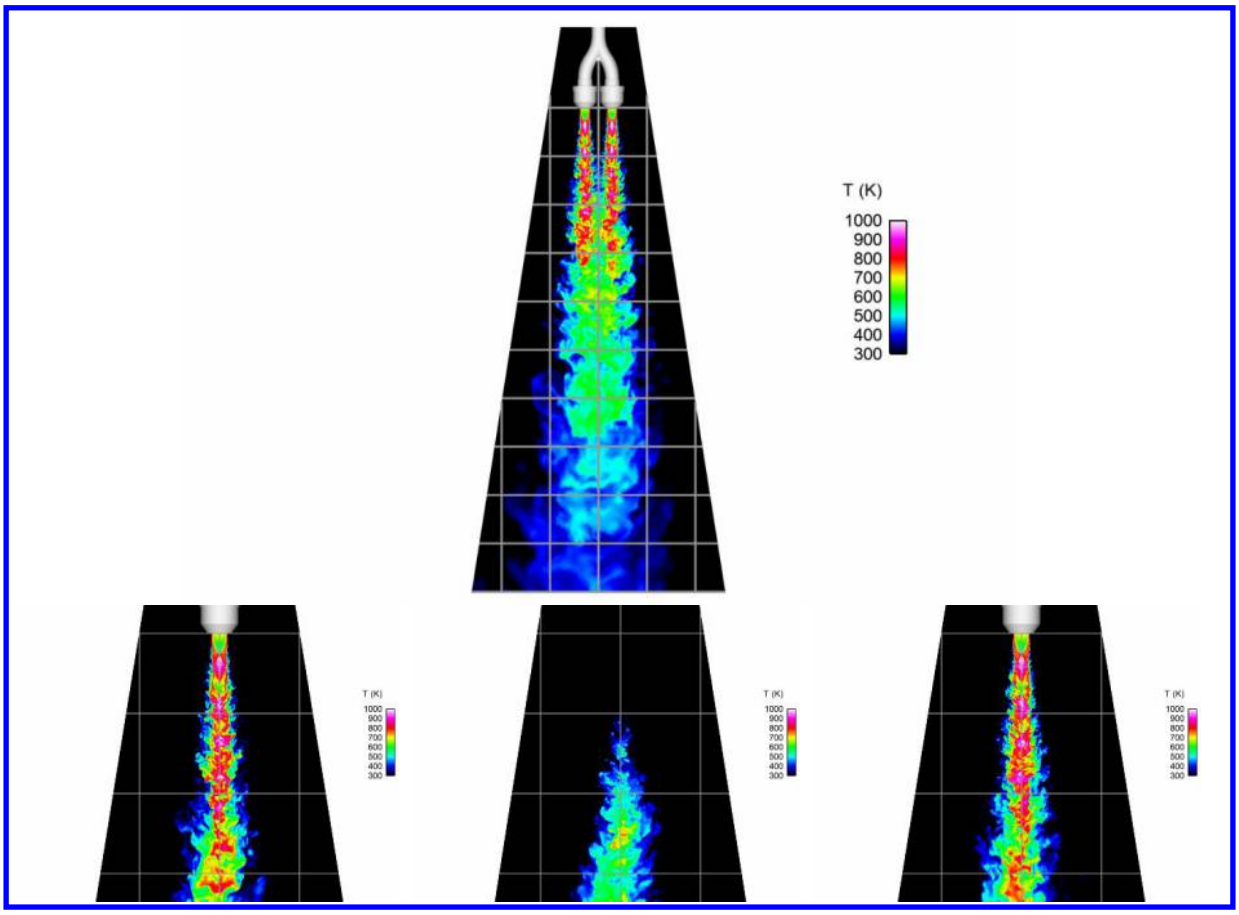

Figure 5: static temperature

(top: jets plane, bottom: midplanes, from left to right: jet 1, symmetry, jet 2)

Figure 5 allows for a global description of the flow: first, near nozzles exit, the jets develops independently. Then, downstream, jets start to merge, as high temperature flow reaches the symmetry midplane. Finally, both jets are combined in one single larger jet.

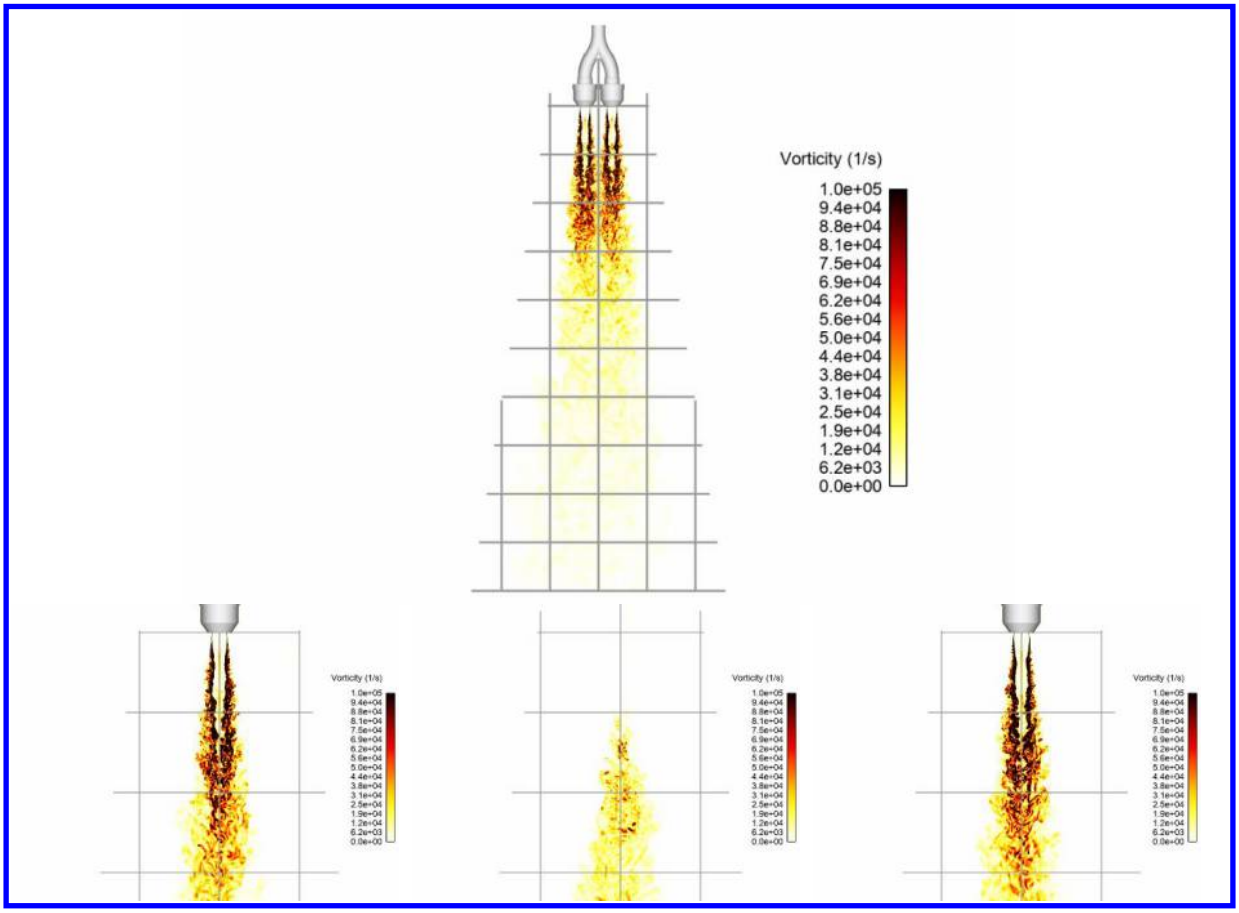

Figure 6: vorticity

(top: jets plane, bottom: midplanes, from left to right: jet 1, symmetry, jet 2)

Figure 6 highlights the shear layer development and the turbulent structures. Due to the geometric triggering in the nozzles, significant levels are found close to the nozzles exit. Moreover, these snapshots validate previous observations regarding the flow structure.

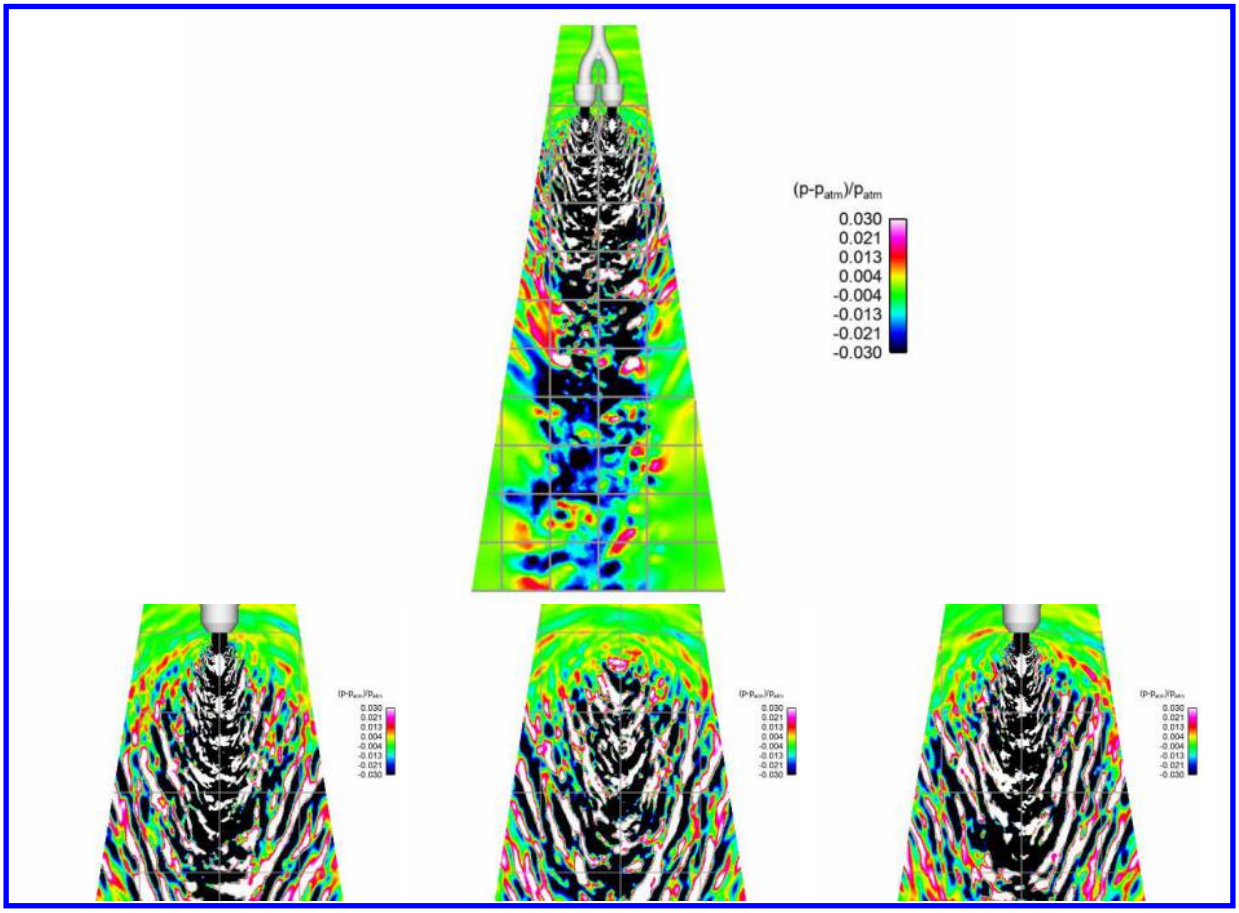

Figure 7: static pressure

(top: jets plane, bottom: midplanes, from left to right: jet 1, symmetry, jet 2)

Finally, static pressure near field is provided in Figure 7. Jet 1 and Jet 2 midplanes display expected emission for a single supersonic jet: high acoustic waves are radiated in the downstream direction (Mach waves), while weaker waves are radiated in the upstream direction. In the symmetry midplane, both strong and weak emissions are also visible, but only starting from merging point. In jets plane, waves are only travelling from one side jets, because each jet shields the emission from the other one. In this plane, it can be noted that Mach wave are mainly emitted in the 20 first D_j.

Mean flow

The axial velocity fields are compared to the PIV data in Figure 8. A zoom close to the nozzles outlet is also available. On each picture, the PIV is on the left and computation is on the right. It must be stated that previous Laser Doppler Velocimetry measurements [32] were performed with slightly higher operating temperature (acoustic conditions) than present PIV and were limited to the first $10D_j$,

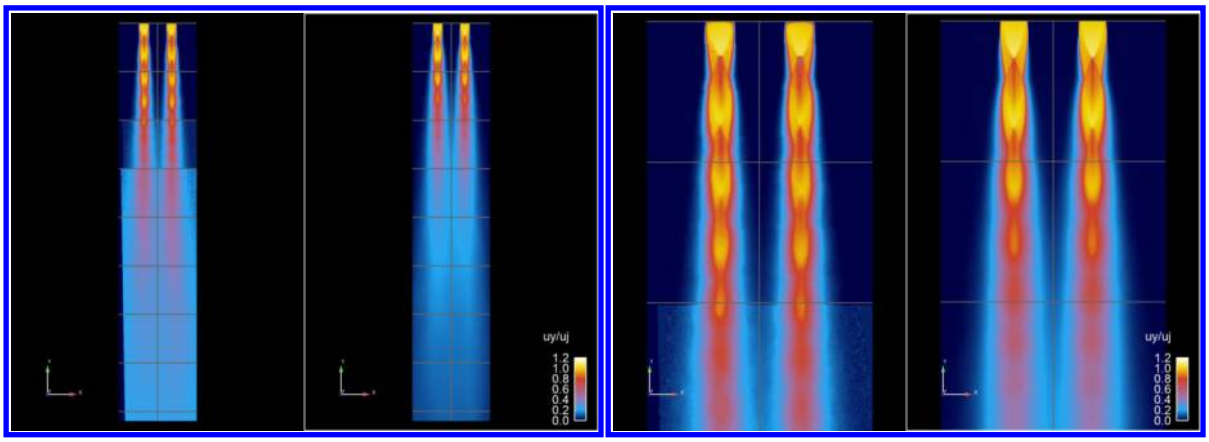

Figure 8: mean axial velocity field (left: whole domain, right: zoom) in jet planes.

For each subfigure: left: PIV, right: computation

Experimental and numerical axial profiles of non-dimensioned axial velocity are plotted along x=-s/2 (jet 1), x=0 (symmetry plane of the jets), x=s/2 (jet 2) in Figure 9, with $s=2.8D_j$ being the jet separation distance.

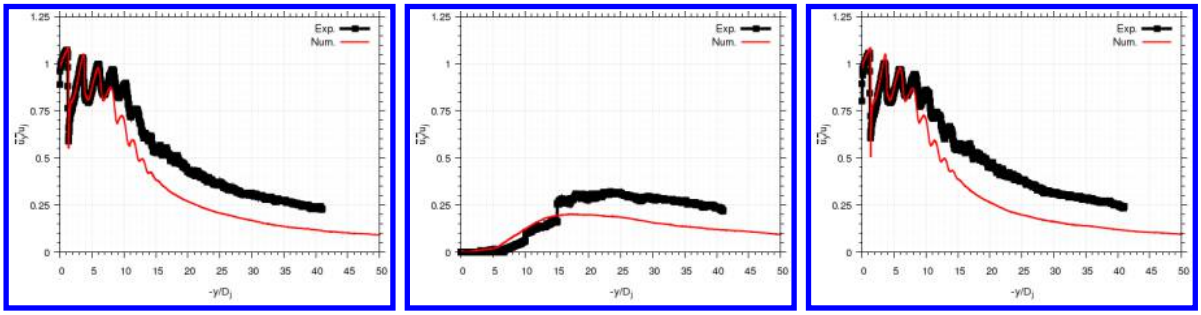

Figure 9: mean axial velocity profiles along axis (from left to right: x=-s/2, x=0, x=s/2)

The comparison of the axial velocity profiles along the axes of the two nozzles shows a very good agreement up to about $8D_j$, whereas after this location, the experiment data show a faster flow than calculated. The experimental profile on the symmetry line (x=z=0) displays a jump at the $10D_j$ position and another one at the $15D_j$ position.

Experimental and numerical radial profiles of non-dimensioned axial velocity are plotted every $2D_j$ spaced axial locations in Figure 10. Horizontal dashed lines highlight nozzles axis.

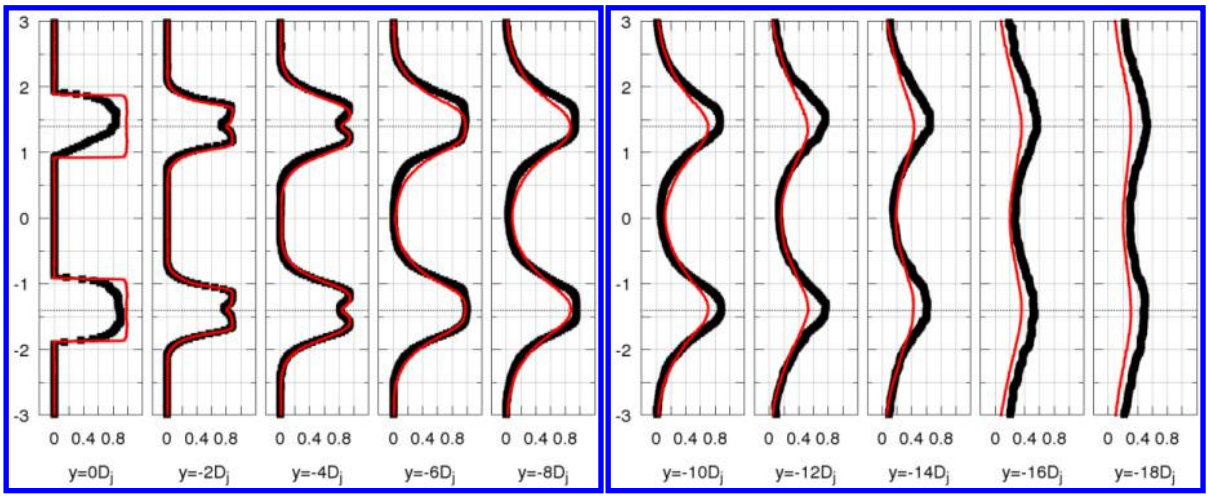

Figure 10: mean radial profiles of axial velocity at different axial locations

It should be noted that at the exit of nozzle 2 (y=0), the PIV shows a dissymmetry of the axial velocity profiles, a behavior not found by the calculation (certainly due to the fact that the same boundary conditions have been applied at the inlet of both nozzles, while T is different experimentally, as indicated in § II). Moreover, at the same position, y=0, the numerical axial velocity mean profiles present a top-hat shape, characteristic of a laminar flow (despite the geometrical triggering in the nozzles), as opposed to the experimental profiles, of parabolic shape, characteristic of a fully turbulent flow. Nevertheless, downstream, the agreement is very good. As noted on the axial profiles, the computational/experimental discrepancy appears around y=-8D$_j$.

Mean fields of turbulent kinetic energy (TKE) are provided Figure 11. As energy is transferred between the turbulent kinetic energy and the sound field, TKE allows first estimation of the approximate distribution of possible acoustic sources in the jet [34].

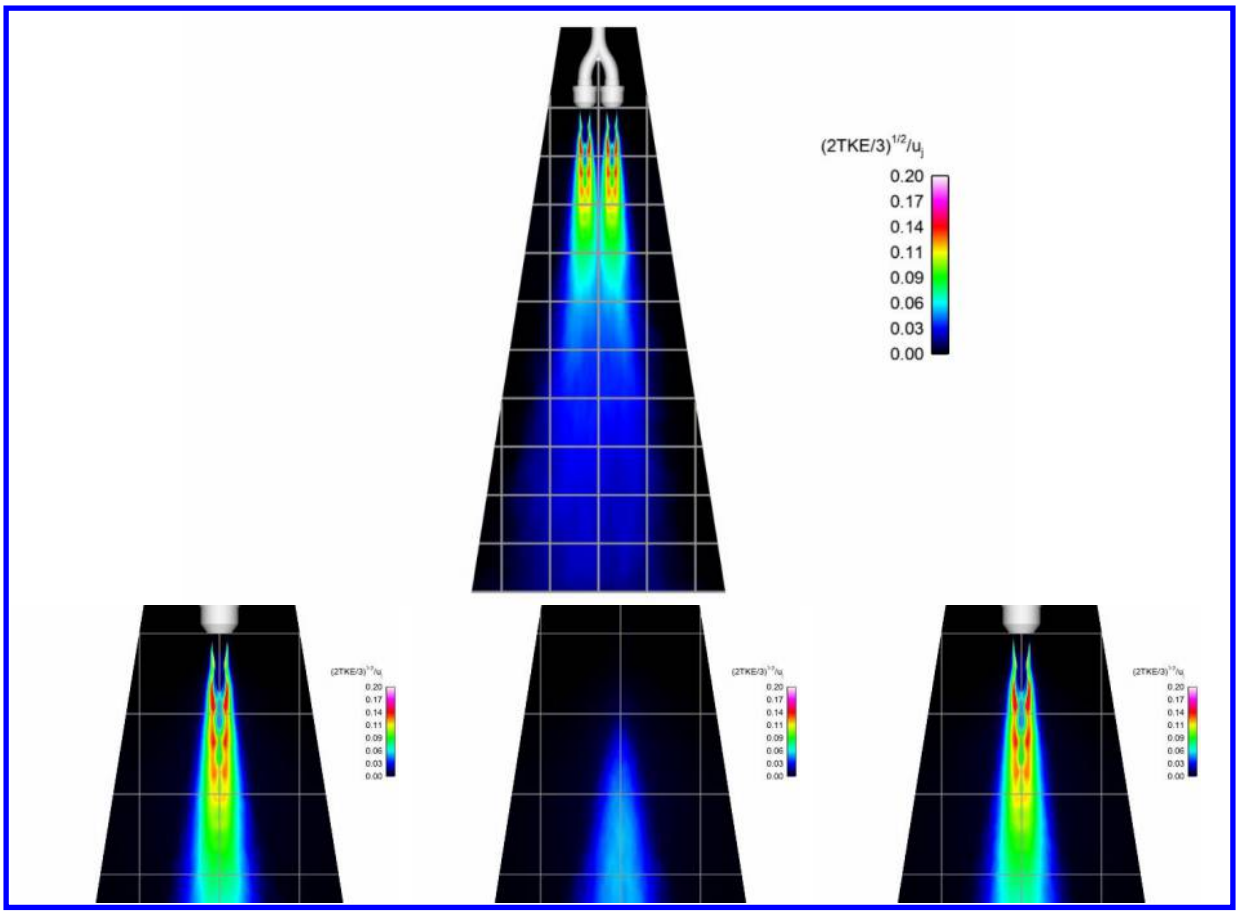

Figure 11: mean turbulent kinetic energy

(top: jets plane, bottom: midplanes, from left to right: jet 1, symmetry, jet 2)

TKE is mainly produced in the jets shear layers, which end merging at about $10D_j$. Moreover, TKE field in the jets plane displays separated contours: there is no major influence of one jet to the other. In the symmetry midplane, lower levels appear from $10D_j$, indicating minor influence.

The root-mean-square (rms) values of the pressure fluctuations are plotted Figure 12. On these maps, the cyan and black lines correspond respectively to iso value of M=1 (supersonic core length) and of V/U_j=0.95 (potential core length). Indeed, potential core length is defined from the jet centerline profiles where the jet velocity is 95% of the exit nozzle velocity, but this criterion only give an insight in this case, because shock cells disrupt the flow.

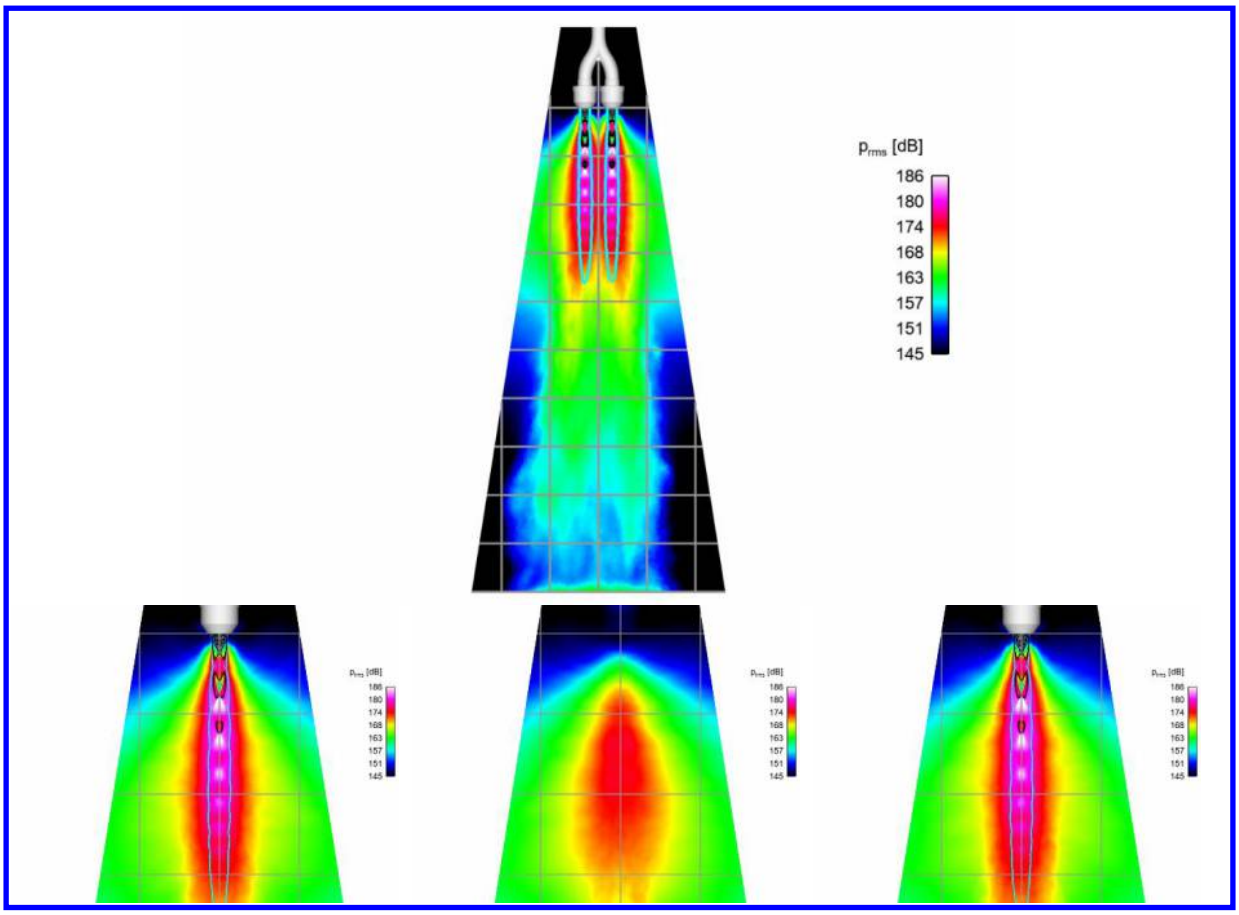

Figure 12: pressure fluctuations

(top: jets plane, bottom: midplanes, from left to right: jet 1, symmetry, jet 2)

When dealing with acoustic power analysis, it has been shown that almost all the power originates from the supersonic portion of the flow and with the distribution peak upstream of the potential core tip [35].

Numerical axial profiles of non-dimensioned axial velocity, non-dimensioned TKE and p_{rms} are plotted along x=-s, x=-s/2, x=0, x=s/2 and x=s in Figure 13.

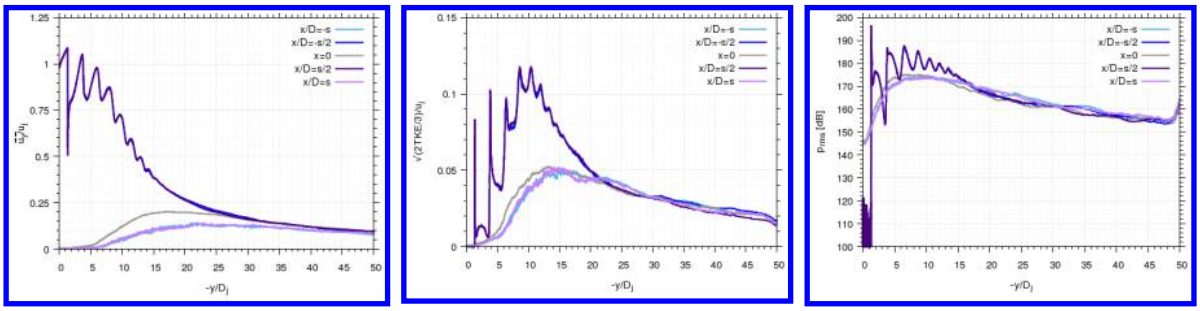

Figure 13: from left to right: axial velocity, TKE, p_{rms} profiles along x=+/- ns (n=0, 1/2, 1)

Looking together at Figure 12 and Figure 13, for single jet, potential core is approximately $6.2D_j$ and supersonic core length is $18D_j$. The higher values of pressure fluctuations are as expected contained in the zone between potential and supersonic cores. However, it can also be noticed that such high value zones are also located

upstream of the second shock cell, near $3.7D_j$, following a lesser value zone being located after the first shock. Such features are also exhibited in the jets plane. In the symmetry midplane, lower but still high values (over 170 dB) are encountered, starting at $3.7D_j$ and ending near $15D_j$. Finally, the flow in this midplane is not supersonic.

Figure 13 also allows the estimation of the twin jets contribution on the center axis with respect to a single jet. The behaviour of the different quantities is globally the same:

- $-y<5D_j$: the curves at x/D_j = -s, 0, s are superimposed; the behaviour for single jet and twin jets is the same, there is no mutual influence of the jets
- $5D_j<-y<25\text{-}30D_j$: the levels increase at $x/D_j = 0$ (twin jets) compared to x/D_j = -s, s (single jet): the two jets interact. However, the effect on the TKE and the p_{rms} is narrower than for axial velocity (up to about $x/D_j = 15$, which correspond to zone between the end of the potential and supersonic cores)
- $-y>25\text{-}30D_j$: the levels reach those at the centre of the single jets: the two jets merge and end up as being a single one

B. Acoustics

Pressure signals are averaged over 12 time windows, leading to a frequency resolution $\Delta St \sim 5\ 10^{-3}$. The averaging of the experimental signals was also adjusted in order to obtain the same ΔSt. The OASPLs will be integrated over the range of St [$5\ 10^{-3}$, 0.35]. The mention "Full" indicates that the OASPLs are integrated throughout the full frequency range. It is recalled that experimental data is obtained for 200K higher operating temperature. Mach waves emission angles are nearly 47° and 63° for the considered jet [6].

Near field microphones

OASPL integrated over the same band for the G3 antenna are reported on Table 1. As G3 sensors are centered on the axis of each nozzle, data is irrelevant at 0° for jet 1 and at 180° for jet 2.

Table 1: OASPL for G3 antenna

Jet	Angle φ (°)	Exp. (dB)	Num. (dB)	Difference (dB)
1	180	140.4	142.9	2.5
2	0	140.4	142.5	2.1
1	90	141.3	143.2	1.9
2	90	141.5	143.6	2.1
1	270	141.9	143.5	1.6
2	270	141.4	143.8	2.4

The computation overestimates the experimental levels by about 2 dB. Computed and experimental difference at given angle (in jets plane or jets midplanes) between jet 1 and jet 2 are always less than 0.5 dB. The data indicates a lower OASPL level at angles 180° (jet 1) and 0° (jet 2) than at angles 90° and 270° (both jets). Drops in OASPL are summarized in Table 2.

Table 2: OASPL drop between jets planes and midplanes

Jet	Angle φ (°)	Exp. drop (dB)	Num. drop (dB)	Difference (dB)
1	180/90	-0.9	-0.3	0.6
1	180/270	-1.5	-0.6	0.9
2	0/90	-1.1	-1.1	0.0
2	0/270	-1.0	-1.3	-0.3

While the experimental drop in OASPL is globally constant (except at 270° for nozzle 1), numerically, it is less pronounced at 180° for jet 1 than at 0° for jet 2. Nevertheless, numerical results exhibit less than 1 dB difference with respect to experimental ones.

The power spectral densities (PSD) of the pressure fluctuations are presented in Figure 14 for jet 1.

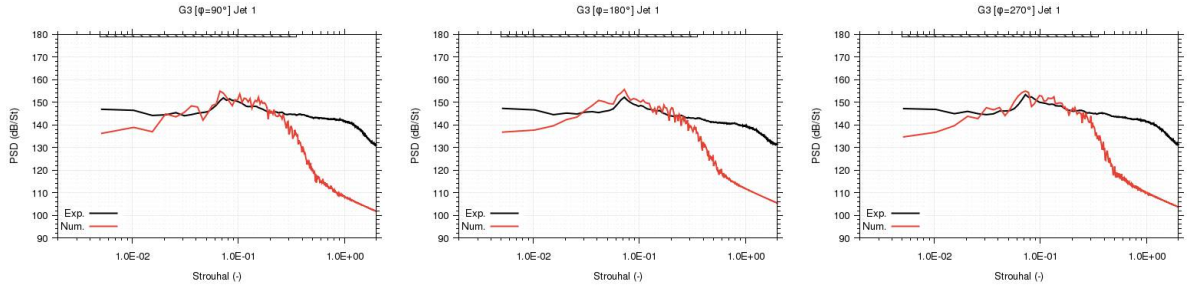

Figure 14: Power spectral densities of the sound pressure levels for G3 (left to right rear midplane, jet plane, front midplane)

The calculation shows a lack of low frequencies, but the agreement is very good in the middle frequencies, mainly around St=0.07 where the maximum level is reached. Main difference between 180° and 90°/270° lies in sharpest peak for jets plane angle, while this peak is flattened for midplane angles. This behavior is also well recovered by computation.

Far field microphones

OASPL for the microphones on the four polar arcs are plotted on Figure 15.

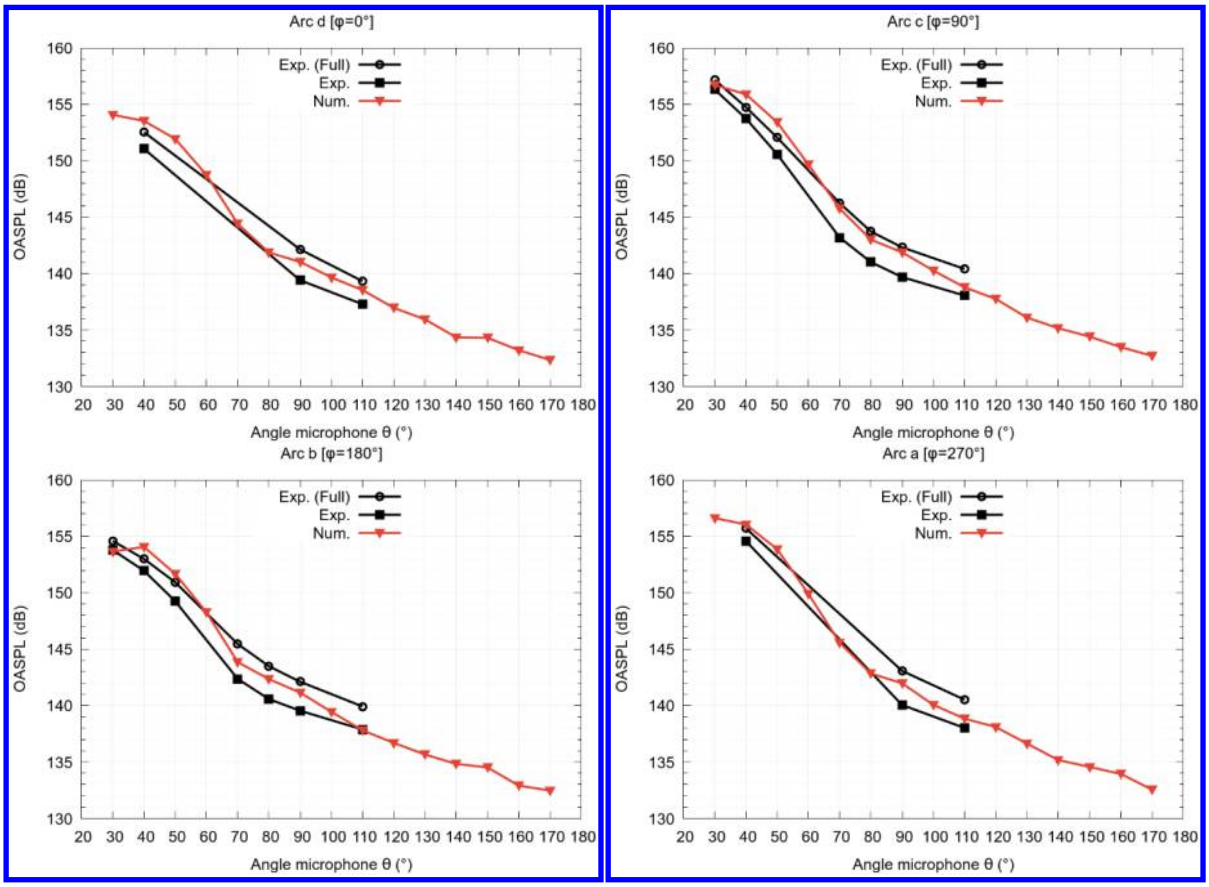

Figure 15: OASPL for the 4 polar arcs

Comparisons are only made for microphones ranging from θ=30° to 110°, where experimental data is available. First, numerical deviation from measurements is at most less than 3 dB at φ=90° and θ=50° and at least 0 dB at φ=180° and θ=110°. Computations always overestimate experience, by about 1.5 dB in average. Experimental trends on independent arcs (OASPL decreasing as angle increases, more quickly before 70-80° than after) are recovered by calculation, except at φ=180° and θ=30°. When looking at φ=0° and 180° (jets plane), experimental and numerical values exhibit less than 1 dB difference. This behavior is also retrieved considering φ=90° and 270° (jet midplanes), with even less than 0.5 dB difference on numerical results. Finally, as expected,

OASPLs at φ=90° or 270° (midplanes) are greater than those at φ=0° or 180° (jets planes), whether considering experimental or numerical results. Table 3 summarizes the difference on OASPL considering perpendicular planes.

Table 3: difference in OASPL (dB) between midplanes and jets plane

	φ=90° vs 0°		φ=90° vs 180°		φ=270° vs 180°		φ=270° vs 0°	
	Exp.	Num.	Exp.	Num.	Exp.	Num.	Exp.	Num.
θ=40°	2.7	2.4	1.8	1.8	2.6	2	3.5	2.5
θ=90°	0.3	0.8	0.1	0.7	0.5	0.8	0.6	0.9
θ=110°	0.8	0.3	0.2	1	0.1	1	0.7	0.3

Some small discrepancies arise when considering one arc or another, but in a general way, difference is high at small angles, decreasing as the latter is increasing. For instance, Figure 16 highlights this behavior for midplane φ=90° and jet 1 plane φ=180°. Except for θ=40° and φ=270°/0°, difference is always less than the theoretically expected 3 dB. It may be the consequence of an interaction effect [22].

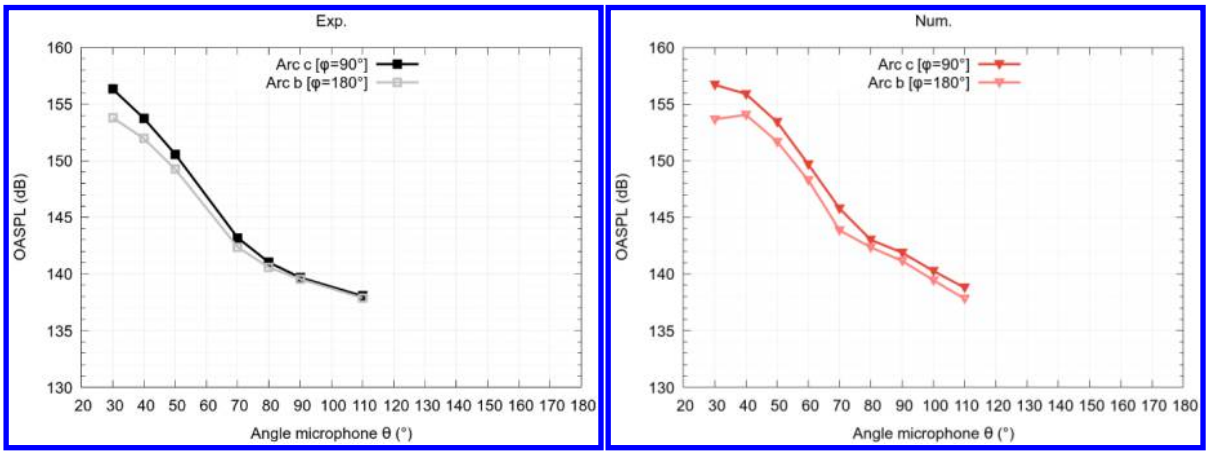

Figure 16: Comparison of OASPLs on 90° and 180° arcs (left: exp.; right: num.)

The power spectral densities (PSD) of the pressure fluctuations are shown in Figure 17 to Figure 19 for jet 1.

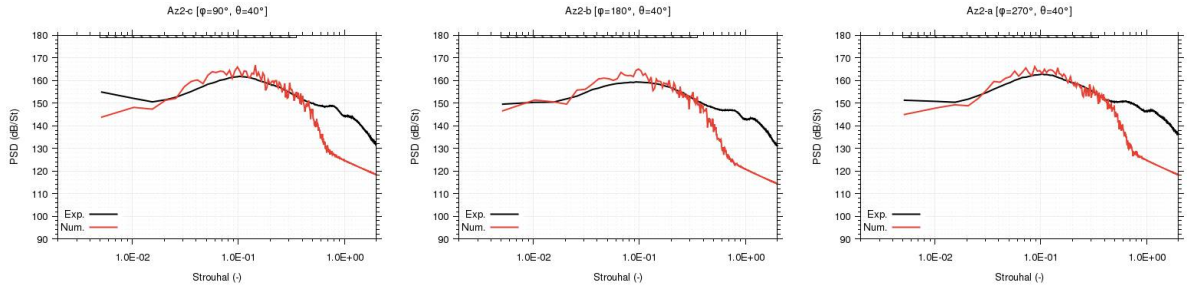

Figure 17: Power spectral densities of the sound pressure levels for 40° angle

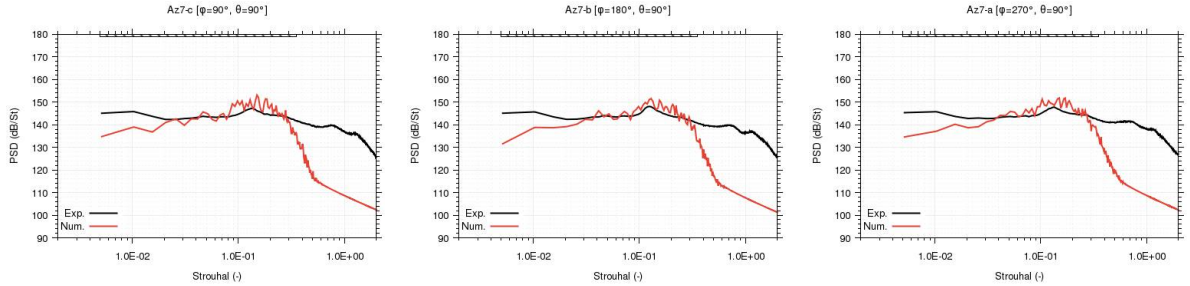

Figure 18: Power spectral densities of the sound pressure levels for 90° angle

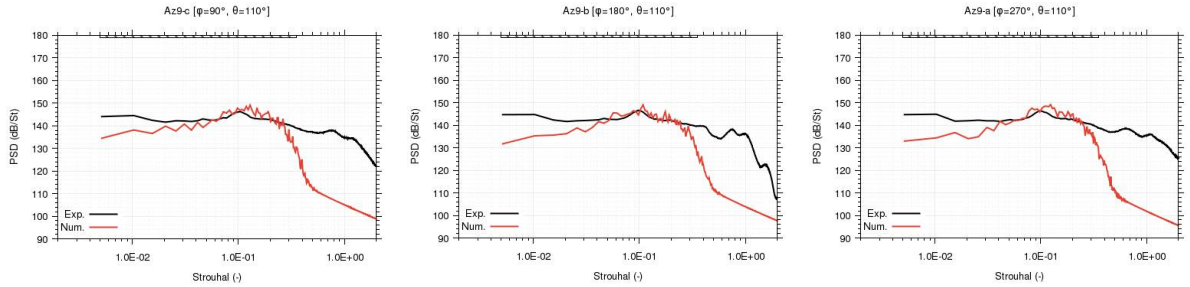

Figure 19: Power spectral densities of the sound pressure levels for 110° angle

The dynamics of the PSDs change with angle θ:

- At low angles (θ=30°-70°), the PSDs exhibit a quite large hump (0.05<St<0.2), whose maximum shifts toward high frequencies (from St=0.09 at θ=30° to St=0.2 at θ=70°), while flattening and contracting. Depending on the angle, the low frequencies decrease while the high frequencies are almost at the same level.
- Around θ=80°-90°, this hump flattens more and more, becoming a peak (St=0.15).
- Then this peak retracts towards lower frequencies as the angle increases (at θ=110°, St=0.1). The low frequencies remain equal, while the high frequencies decrease.

The influence of considering φ=90°/270° arcs ("2 jets") compared to φ=0°/180° arcs ("1 jet") only results in an increase of the bump levels, thus at low angles. At higher angles, around θ=90° and the appearance of the peak, there is no more influence of the "2 jets". This phenomenon was already visible on the OASPL.

These comments are valid whether we consider experimental or numerical signals, although due to a lower available time, the corresponding computed DSPs are noisier.

The agreement in the mid frequencies is globally good. The calculation shows a lack of low frequency (not very detrimental) and a cutoff frequency that is perhaps still a little low to capture the phenomena appearing between θ=60° and 90°, when the maximum of PSD moves towards the high frequencies.

Plots of OASPLs for the microphones on the two far field G4 and G5 antennas are displayed on Figure 20. Note that 315° experimental microphone on G5 seems out of order and is then not presented.

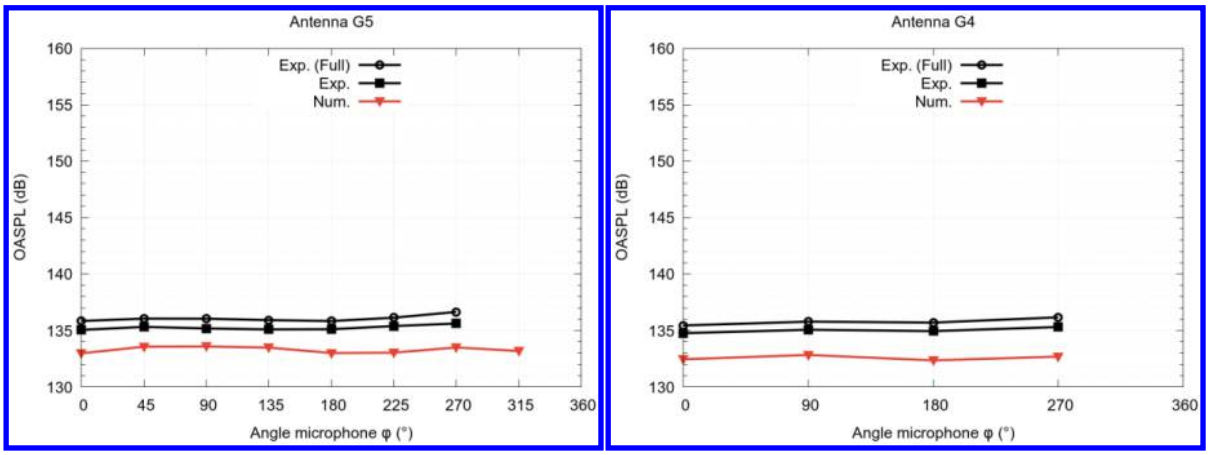

Figure 20: Comparison of OASPLs on far field antennas (left: G5; right: G4)

On these antennas, numerical underestimation is ranging from 1.6 to 2.4 dB for G5, and about 2.5 dB for G4: the levels are more underestimated by the computation as we move upstream from the nozzle exit. Globally, at these locations, shielding effects are not present, as OASPLs are very close at all angles, with no marked effect between midplanes and jets plane. Furthermore, G4 microphones at φ=0, 90, 180 and 270° are near θ=170° microphone on arc d, c, b and a, respectively. Therefore, when comparing numerical levels obtained on G4 with those on arcs at same φ angles, levels are found very close (about 0.1 dB), suggesting that extended trends on Figure 15 are well reproduced. Transition between numerical overestimation to underestimation is then evaluated after 110° at $r=25D_j$. As for these sensors grid resolution is similar, and order mapping set to 4^{th} order, it may be due to the vicinity of the body motor as outer shape of the model is not faithfully reproduced in computation.

The power spectral densities (PSD) of the pressure fluctuations are plotted in Figure 17 for half of G4 antenna.

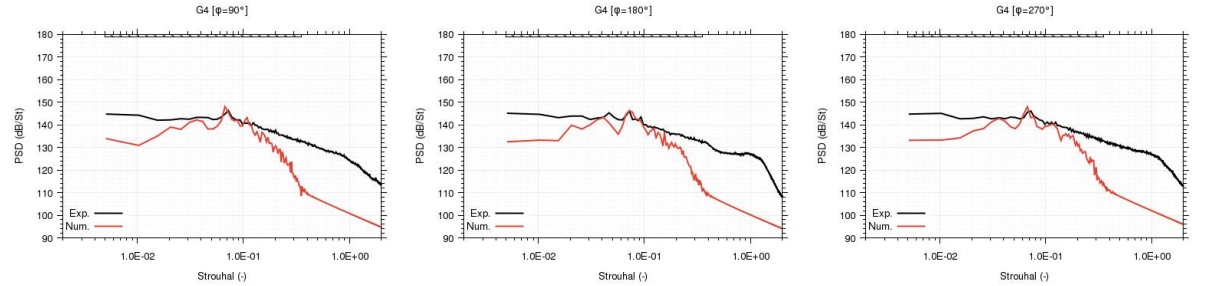

Figure 21: Power spectral densities of the sound pressure levels for G4 (left to right rear midplane, left barrel plane, front midplane)

The trends are the same as for G3 (see Figure 14): low frequencies are underestimated and peak around St=0.07 is well recovered, with the difference that the calculation cuts earlier, which can explain the underestimation of the OASPL on G4. Despite the previous comment on similarity of OASPLs on all angles, a smaller peak is observed at 180° at Strouhal ~0.035, which is not present at perpendicular angles. Conversely, computation displays such peak at all angles, but being more marked also at 180°. Overall, computations agree well with experimental results.

VI. Conclusion

Main numerical characteristics of this study regarding the evaluation of noise radiated by free hot supersonic twin jets relies on the following two major points. On the one hand, on the geometrical triggering of turbulence in the convergent nozzles for LES part computing the acoustic sources, and on the other hand, on the use of a high order CAA code, fully coupled with the CFD code, allowing propagating the possible nonlinear acoustic waves from the jet near field to the microphones in the far field, at a lower cost. Moreover, particular attention has been paid to the generation of the mesh, whether in the nozzle (in order to optimize the presence of the triggering step, the treatment of the walls or the azimuthal resolution at the exit), or in the jet itself. This combination of meshing and numerical adjustments helped us to build a validated methodology applicable to jet aeroacoustics configurations.

It allowed us to obtain very satisfactory results. Indeed, the numerical aerodynamic profiles show a good agreement with the PIV for several diameters downstream from the nozzle exit. Further downstream, the agreement is less good,that will be further investigated in future work. It will be necessary to verify these before

concluding. Note that the numerical choice to apply identical boundary conditions to both nozzles deviate from the real experimental conditions. The aerodynamic results show that the interactions between the two jets only occur several diameters after the nozzle exit.

Regarding the acoustics, results are very encouraging. Around the nozzle (G3), the numerical signals show an overestimation of at most 2 dB on these microphones. On the far field arcs, this overestimation varies between 0 and 3 dB. However, on far field antennas around the generator, numerical results underestimate experimental one by at most 2.5 dB. However, when looking at far field arcs, it appears that the transition between levels overestimation and underestimation is located around 110°. It seems to be related to a too low mesh cutoff frequency at upstream position, or to an inaccurate reproduction of the external shape of the generator. Power spectral densities analysis reveals different behaviors along the arcs, on the mid-frequency range of the frequency domain. Indeed, at low angles, PSD exhibit an energetic bump around St~0.1. When angle increases, to 90°, this bump concentrates into one peak near St=0.15. Then, at 110°, this peak retracts to St=0.1. Even higher, at 170° (in the vicinity of the generator), this peak finally retracts again to St=0.07 (same as for near field microphones around the generator). It can be deduced that acoustic phenomena or intensity involved are different according to the considered locations, probably strong Mach waves at lower angles and lighter shock-associated noise at high angles.

Finally, it must be pointed out that it is expected that microphones located in the plane containing the 2 jets (*i.e.* azimuth 0° and 180°) receive the emission for only one jet (due to the shielding effect) and conversely that microphones located in the mid plane perpendicular (*i.e.* azimuth 90° and 270°) receive the emission for both jets (interaction effect). This behavior is well recovered by the computation. Furthermore, in that latter plane, acoustic power addition is expected to be 3 dB. Experimental and numerical higher levels (localized at low angles) do not correspond exactly to this theoretical addition, suggesting that some acoustic sources may have been reduced by a possible mixing effect. At 90° and higher angles, differences in the levels are less marked, indicating that acoustics of the two jets do not add up, because of a single merged jet emission.

Acknowledgments

This study is supported by the French space agency CNES and ONERA's scientific direction. Special acknowledgments are addressed to H. Lambaré, research scientist at CNES and technical referee regarding the acoustic environment of rocket launchers. The authors are grateful to S. Piantanida, R. Bouju and P. Berterretche from Pprime Institute for providing experimental data.

References

[1] Brès, G., Lele, S., "Modelling of jet noise: a perspective from large-eddy simulations," Philosophical Transactions of the Royal Society A, Vol. 377, No. 20190081, 2019.
doi: 10.1098/rsta.2019.0081

[2] Lubert, C.P., Gee, K.L., and Tsutsumi, S., "Supersonic jet noise from launch vehicles: 50 years since NASA SP-8072", The Journal of the Acoustical Society of America, vol. 151, p. 752, 2022.
doi: 10.1121/10.0009160

[3] C.K.W Tam, N.N. Pastouchenko, and K. Viswanathan., "Fine-Scale Turbulence Noise from Hot Jets". AIAA Journal, 43(8):1675–1683, 2005.
doi: 10.2514/1.8065

[4] Kantola, R.A., "Acoustics Properties Of Heated Twin Jets", Journal of Sound and Vibration, vol. 79, no. 1, pp. 79-106, 1981.

[5] Simonich, J.C., Amiet, R.K., and Schlinker, R.H., "Jet Shielding of Jet Noise", NASA Contractor Report 3966, 1986.

[6] Norum, T.D. and Shearin, J.G., "Dynamic loads on twin jet exhaust nozzles due to shock noise", Journal of Aircraft, vol. 23, no. 9, 1986.
doi: 10.2514/3.45370

[7] Seiner, J.M., Manning, J.C., and Ponton, M.K., "Dynamic Pressure Loads Associated with Twin Supersonic Plume Resonance", AIAA Journal, vol. 26, no. 8, pp. 954-960, 1986.
doi: 10.2514/3.9996

[8] Wlezien, R.W., "Nozzle geometry effects on supersonic jet interaction", AIAA Journal, vol. 27, no. 10, 1989.
doi: 10.2514/3.10272

[9] Shaw, L., "Twin-jet screech suppression", Journal of Aircraft, vol. 27, no. 8, 1990
doi: 10.2514/3.25344

[10] Walker, S., "Twin jet screech suppression concepts tested for 4.7 percent axisymmetric and two-dimensional nozzle configurations", 26th Joint Propulsion Conference, Orlando, FL: AIAA 2150, 1990.
doi: 10.2514/6.1990-2150

[11] Alkislar, M.B., Krothapalli, A., Choutapalli, I., and Lourenco, L., “Structure of Supersonic Twin Jets”, AIAA Journal, vol. 43, no. 11, 2005.
doi: 10.2514/1.10431

[12] Raman, G., Panickar, P., and Chelliah, K., “Aeroacoustics of twin supersonic jets: a review”, International Journal of Aeroacoustics, vol. 11, no. 7&8, pp. 957-984, 2012.
doi: 10.1260/1475-472X.11.7-8.957

[13] Moustafa, G.H., “Interaction of Axisymmetric Supersonic Twin Jets”, AIAA Journal, vol. 33, no. 5, pp. 871-875, 1995.
doi: 10.2514/3.12508

[14] Bozak, R. and Henderson, B., “Aeroacoustic Experiments with Twin Jets”, 17th Aeroacoustics Conference, Portland, OR: AIAA/CEAS-2790, 2011.
doi: 10.2514/6.2011-2790

[15] Ozawa, Y, Nonomura, T., Saito, Y., and Asai, K., “Aeroacoustic Fields of Supersonic Twin Jets at the Ideally Expanded Condition”, Trans. Japan Soc. Aero. Space Sci., vol. 64, no. 6, pp. 312-324, 2021.
doi: 10.2322/tjsass.64.312

[16] Kuo, C.-W., Cluts, J., and Samimy, M., “Exploring Physics and Control of Twin Supersonic Circular Jets”, AIAA Journal, vol. 55, no. 1, pp. 68-85, 2017.
doi: 10.2514/1.J054977

[17] Knast, T., Bell, G., Wong, M., Leb, C.M., Soria, J., Honnery, D. R., and Edgington-Mitchell, D., “Coupling Modes of an Underexpanded Twin Axisymmetric Jet”, AIAA Journal, vol. 56, no. 9, pp. 3524-3535, 2018.
doi: 10.2514/1.J056434

[18] Bell, G., Cluts, J., Samimy, M., Soria, J., and Edgington-Mitchell, D., “Intermittent modal coupling in screeching underexpanded circular twin jets”, J. Fluid Mech., vol. 910, no. A20, 2021.
doi: 10.1017/jfm.2020.909

[19] Goparaju, K. and Gaitonde, D.V., “Dynamics of Closely Spaced Supersonic Jets”, Journal of Propulsion and Power, vol. 34, no. 2, pp. 327-339, 2018.
doi: 10.2514/1.B36648

[20] Gao, J., Xu, X., and Li, X., “Numerical Simulation of Supersonic Twin-Jet Noise with High-Order Finite Difference Scheme”, AIAA Journal, vol. 56, no. 1, pp. 290-300, 2018.
doi: 10.2514/1.J055751

[21] Ahn, M.-H., Lee, D.-J., and Mihaescu, M., “A numerical study on near-field pressure fluctuations of symmetrical and anti-symmetrical flapping modes of twin-jet using a high-resolution shock-capturing scheme”, Aerospace Science and Technology, vol. 119, no. 107147, 2021.
doi: 10.1016/j.ast.2021.107147

[22] Pineau P., Bogey C., “Acoustic shielding and interaction effects for strongly heated supersonic twin jets”, AIP Advances 11, 075114, 2021.
doi: 10.1063/5.0059789

[23] Lambaré, H. “Experimental study of the aeroacoustic interaction between two supersonic hot jets”, J. Acoust. Soc. Am. 142, 2490, 2017
doi: 10.1121/1.5014088

[24] Langenais A., Vuillot F., Troyes J., Lambaré H. “Computation of the noise radiated by a hot supersonic jet deflected in a flame trench”, J. Acoust. Soc. Am. 149 (3), 2021
doi: 10.1121/10.0003759

[25] Langenais A., Vuillot F., Troyes J., Bailly C. “Accurate simulation of the noise generated by a hot supersonic jet including turbulence tripping and nonlinear acoustic propagation”, Phys. Fluids 31, 016105, 2019
doi: 10.1063/1.5050905

[26] Gely, D., Valière, J.-C., Lambaré, H., and Foulon, H., ”Overview of aeroacoustic research activities in MARTEL facility applied to jet noise”, INTER-NOISE and NOISE-CON Congress and Conference Proceedings, 1282-1290, 2006.

[27] Piantanida, S., Berterretche, P. “Acoustic characterisation of two parallel supersonic jets”, InterNoise, 2019.

[28] Troyes, J., Vuillot, F., Lambaré, H., and Espinosa Ramos, A. “Numerical Study of Free Supersonic Hot Jet on Unstructured Grids with Emphasis on Aerodynamics and Resulting Radiated Noise”, 22nd Aeroacoustics Conference, Lyon, France: AIAA/CEAS-2734, 2016.
doi:10.2514/6.2016-2734

[29] Refloch A., Courbet B., Murrone A., Villedieu P., Laurent C., Gilbank P., Troyes J., Tessé L., Chaineray G., Dargaud J.-B., Quémerais E, Vuillot F., “CEDRE software”, Aerosp. Lab J. 2, AL02-11, 2011

[30] Scherrer D., Chedevergne F., Grenard P., Troyes J., Murrone A., Montreuil E., Vuillot F., Lupoglazoff N., Huet M., Sainte-Rose B., Bertier N., Lamet J.-M., Le Pichon T., Radenac E., Nicole A., Matuszewski L., Errera M.-P., “Recent CEDRE applications”, Aerosp. Lab J. 2, AL02-13, 2011

[31] Delorme P., Mazet P., Peyret C., Ventribout Y., “Computational aero-acoustics applications based on a discontinuous Galerkin method”, C.R. Méc. 333(9), 676-682, 2005
doi: 10.1016/j.crme.2005.07.007

[32] Troyes J., Vuillot F., Langenais A., Lambaré H., "Coupled CFD-CAA Simulation of the Noise Generated by a Hot Supersonic Jet Impinging on a Flat Plate with Exhaust Hole", 25th Aeroacoustics Conference, Delft, The Netherlands:

AIAA/CEAS-2752, 2019.
doi: 10.2514/6.2019-2752

[33] Quémerais E., “Coupling with interpolation parallel interface”, ONERA web site, 2016.
https://w3.onera.fr/cwipi/ (Last viewed 14 January 2022).

[34] Chakrabarti, S., Gaitonde, D.V., Unnikrishnan, S.N., Stack, C., Baier, F., Karnam, A., and Gutmark, E. “Turbulent Statistics of a Hot, Overexpanded Rectangular Jet”, Journal of Propulsion and Power, 38(3):421-436, 2022
doi: 10.2514/1.B38073

[35] Leete K.M., Gee K.L., Liu J., Wall A.T. “Near-field acoustical holography and acoustic power analysis of a simulated, highly heated supersonic jet”, The Journal of the Acoustical Society of America 151, 1989, 2022
doi: 10.1121/10.0009827